Electrochimica Acta 55 (2010) 7290–7297

Contents lists available at ScienceDirect

Electrochimica Acta

journal homepage: www.elsevier.com/locate/electacta

Partially oxidized niobium carbonitride as a non-platinum catalyst for the reduction of oxygen in acidic medium

Kyung-Don Nam[a], Akimitsu Ishihara[a,*], Koichi Matsuzawa[a], Shigenori Mitsushima[a], Ken-ichiro Ota[a,1], Masashi Matsumoto[b], Hideto Imai[b]

[a] Chemical Energy Laboratory, Yokohama National University, 79-5 Tokiwadai, Hodogaya-ku, Yokohama, Kanagawa 240-8501, Japan
[b] Green Innovation Laboratories, NEC Corporation, 34 Miyukigaoka, Tsukuba, Ibaraki 305-8501, Japan

ARTICLE INFO

Article history:
Received 6 May 2010
Received in revised form 10 July 2010
Accepted 17 July 2010
Available online 23 July 2010

Keywords:
Niobium oxide
Niobium carbonitride
Non-platinum cathode
Polymer electrolyte fuel cell
Oxygen reduction reaction

ABSTRACT

Partially oxidized $NbC_{0.5}N_{0.5}$ has been evaluated as a non-platinum catalyst for the reduction of oxygen in acidic medium. $NbC_{0.5}N_{0.5}$ powder was partially oxidized in N_2 gas containing O_2 of 10^{-4} atm at the temperature range of 700–1000 °C. Partially oxidized $NbC_{0.5}N_{0.5}$ had a definite oxygen reduction reaction (ORR) activity, while as-prepared $NbC_{0.5}N_{0.5}$ and completely oxidized Nb_2O_5 had a poor catalytic activity for ORR. The onset potential of the partially oxidized $NbC_{0.5}N_{0.5}$ for the ORR achieved 0.92 V vs. RHE in 0.1 M H_2SO_4 at 30 °C. The results of X-ray absorption spectroscopy and ionization potential measurements suggested that oxygen-vacancy defects might be responsible for the oxygen reduction capability by creating electronically favorable oxygen adsorption sites.

1. Introduction

Polymer electrolyte fuel cells (PEFCs) are expected as power sources for residential and transport applications due to their high theoretical efficiency of energy conversion, high power density, and low operating temperature. However, PEFCs have some serious problems to be solved before wide commercialization. In particular, a large overpotential of oxygen reduction reaction (ORR) must be reduced in order to obtain high energy efficiency. Although Pt is generally used as a cathode catalyst in the present PEFCs, its catalytic activity for the ORR is insufficient to obtain the required efficiency [1,2]. Other issues regarding Pt usage are its high cost and limited resources. Considering an application to fuel cell vehicles, the natural resource of Pt is insufficient. Therefore, many attempts, such as a greater dispersion of Pt particles and/or an alloying with transition metals, have been made to reduce Pt utilization. However, because dissolution of highly dispersed Pt particles and oxidation of a support carbon became important issues for long-time operation in recent years, a drastic reduction of the Pt utilization seemed difficult. Therefore, development of a stable non-platinum catalyst is vital [3,4]. Many studies have been performed to develop non-platinum cathode catalysts for low-temperature fuel cells. Organometallic complexes and chalcogenides were famous as candidates for the alternative Pt catalysts.

Jasinski firstly introduced a cobalt phthalocyanine as an electrocatalyst for the ORR in 35% KOH in 1964 [5]. Jahnke and Schonborn applied transition metal phthalocyanines to the non-Pt cathode catalysts in 4.5N H_2SO_4 in 1969 [6]. Many organometallic complexes have been widely investigated since then [7,8]. Bashyam and Zelenay showed that the cobalt–polypyrrole composite catalyst enabled power densities of about 0.15 W cm^{-2} in H_2–O_2 fuel cells and displayed no signs of performance degradation for more than 100 h [9]. In recent years, Lefevre et al. reported that iron-based catalysts exhibited the similar performance of platinum supported carbon although the catalyst loading was much greater than that of Pt [10]. However, these catalysts have poor stability in an acid media such as H_2SO_4 and polymer electrolytes.

Alonso-Vante and Tributsch found that $Mo_{4.2}Ru_{1.8}Se_8$ had a catalytic activity for the ORR in acidic media in 1986 [11]. Alonso-Vante and co-workers reported that Ru acted as active site and Ru metal was protected against oxidation to Ru oxides by the chalcogens additives [12]. RuSe, RuTe, MoReSe, MoRhS, MoOsS, MoSe, ReRuS, IrRuS, (RuMo)SeO, WRuSe, RhS, RhSe, RuCrSe, RuFeSe, and CoSe were investigated besides MoRuSe [13]. Because these chalcogenides were inactive for methanol, the development for cathodes as direct methanol fuel cells was examined. However, Ru and Rh are precious metals and their resources are very limited. Therefore, the development of a new non-platinum catalyst is strongly required.

* Corresponding author. Tel.: +81 45 339 4022; fax: +81 45 339 4024.
E-mail address: a-ishi@ynu.ac.jp (A. Ishihara).
[1] ISE member.

0013-4686/$ – see front matter © 2010 Elsevier Ltd. All rights reserved.
doi:10.1016/j.electacta.2010.07.048

It was reported that tungsten carbide with tantalum addition [14], tantalum oxynitride [15–18], zirconium oxide [19–21], titanium oxide [22], zirconium oxynitride [23–25], chromium carbonitride [26] and tantalum carbonitride [27] were stable in an acid solution and had a definite catalytic activity for the ORR. In particular, we found that the partially oxidized tantalum carbonitride powder had a definite catalytic activity for the ORR and the mixture with the carbon black as a current collector was useful to increase the ORR current [28–30]. We summarized these oxide-based non-platinum catalysts [31].

Niobium belongs to the same group of tantalum, that is, 5 group metal. Resource of niobium, 4.4×10^3 kton, is two orders of magnitude greater than that of platinum, 37 kton [3]. We found that a partially oxidized niobium carbonitride powder had a definite catalytic activity for the ORR [32]. However, the characterization of the specimens and the discussion of the correlation between the physical properties and the catalytic activity for the ORR had not sufficiently performed yet.

In this study, niobium carbonitride as a starting material was synthesized by a mixture of metal Nb and carbon powder. A partial oxidation of niobium carbonitride was performed to obtain different surface state by heat treatment in N_2 gas containing low oxygen partial pressure. Partially oxidized specimens were characterized using X-ray diffraction, X-ray photoelectron spectroscopy, X-ray absorption spectroscopy and ionization potential analyses to discuss the correlation between ORR activity and physico-chemical properties.

2. Experimental

2.1. Electrocatalyst preparation

Niobium carbonitride (NbC_xN_y) powder was synthesized by using a mixture of Nb powder (<45 μm, 99.9%, High purity chemicals, Japan) and carbon black (average particle size <1 μm, 99.95%, SEC Corp.). The Nb and carbon black powders were uniformly mixed. A cylindrical shaped tablet (10 mm Ø × 5 mm) of their mixed powder was made by uni-axial pressing at 2 MPa, and then the tablet was heat-treated in an alumina tube furnace in N_2 atmosphere at 1500 °C for 10 h. The composition of NbC_xN_y powder was controlled by the molar ratio of mixing carbon black. In this study, $NbC_{0.5}N_{0.5}$ powder was used as a starting material. The composition was determined by Vegard's law [33]. $NbC_{0.5}N_{0.5}$ powders were heat-treated in low pressure of oxygen to examine the effect of the partial oxidation on the catalytic activity for the ORR. The heat treatment was firstly carried out in a quartz tube with N_2 gas containing O_2 of 10^{-4} atm O_2 at the temperature range of 700–1000 °C with holding time of 20 h. Then, the partial oxidation was performed with N_2 gas containing O_2 of 10^{-4} atm O_2 at 900 °C with the holding time from 20 to 50 h. The partially oxidized $NbC_{0.5}N_{0.5}$ powder was expressed as Nb-CNO in this paper. Nb_2O_5 was prepared by heat-treatment with N_2 gas containing O_2 of 10^{-3} atm O_2 at 900 °C to compare the ORR activity.

2.2. Electrochemical measurements

In order to evaluate the catalytic activity for the ORR and the electrochemical stability, the working electrode was prepared as follows. The $NbC_{0.5}N_{0.5}$ with and without heat treatment powders and Ketjen Black (5 wt.%) were mixed, and the mixture was suspended in a mixture of 1-propanol and distilled water. The suspension was evenly dropped onto the glassy carbon rod (5.2 mm Ø). The catalyst loading was about 5 mg on the glassy carbon rod. Dilute Nafion® solution (0.5 wt.%), then, was dropped onto the surface. The coated glassy carbon rod was dried in inert atmosphere at 120 °C for 1 h with a drying oven to prepare a working electrode. Electrochemical measurements were carried out in 0.1 mol dm^{-3} H_2SO_4 at 30 °C in N_2 and O_2 using a three-electrode cell. A reversible hydrogen electrode (RHE) and the carbon plate were used as a reference and counter electrode, respectively. In order to examine the electrochemical stability, cyclic voltammetry (CV) was carried out from 0.05 to 1.0 V vs. RHE in N_2 at a scan rate of 50 mV s^{-1}. When cyclic voltammetry reached a steady state, slow scan voltammetry (SSV) was measured from 0.2 to 1.0 V vs. RHE in N_2 and O_2 at a scan rate of 5 mV s^{-1} to obtain the potential–current curves for the ORR. The difference between the current under O_2 (i_{O_2}) and that under N_2 (i_{N_2}) was corresponded to the oxygen reduction current (i_{ORR}), that is, $i_{ORR} = i_{O_2} - i_{N_2}$. The current density was based on the geometric area of the working electrode. The onset potential for the ORR, E_{ORR}, was defined as the electrode potential at the $i_{ORR} = -0.2$ μA cm^{-2}. The onset potential and the i_{ORR} at 0.6 V were utilized to evaluate the catalytic activity for the ORR in this study.

2.3. Characterization

The crystalline structures of the Nb-CNO specimens were characterized by using powder X-ray diffraction measurements (XRD-6000, Shimadzu) with Cu Kα radiation (λ = 0.15406 nm) in the 2 range from 10° to 80°. The surface morphology was examined by field emission scanning electron microscope (FE-SEM, Carl Zeiss ULTRA 55). X-ray photoelectron spectroscopy (XPS Quantera SXM, PHI) was utilized to analyze chemical bonding states of the surface. The local structures around Nb atoms were also characterized by X-ray absorption spectroscopy. XAS was suitable for analyzing the catalytic properties of materials since it probes both structural and electronic structural information from the extended fine-structure (EXAFS) and near-edge structure (XANES), respectively. To obtain structural information of the surface phase, we used conversion-electron-yield (CEY) XAS in addition to the conventional transmission XAS [34]. Since the CEY-XAS detects the flux of He^+ ions produced by the electrons emitted from the near surface regions due to an Auger process, we can selectively analyze that local structure of near surface phases restricting the probing depth within the escape depth of the Auger electrons [35]. The probing depth of CEY-XAS for an Nb-K edge was estimated to be 195 nm for Nb_2O_5 (density: 4.47 g cm^{-3}) by using the Schroeder formula [36]. An ionization potential of the specimens was measured using a photoelectron spectrometer surface analyzer (Model AC-3, Riken Keiki) [37].

3. Results and discussion

3.1. Crystal structure and surface morphology

Fig. 1 shows the XRD patterns of NbC_xN_y with and without heat-treatment under N_2 gas containing O_2 of 10^{-3}–10^{-4} atm O_2 at the temperature range of 700–1000 °C. As shown in Fig. 1(a), NbC_xN_y, which was carbonitrided from the mixture of metal Nb and carbon black powders, was synthesized without any other secondary phase such as metallic Nb, Nb_2C and β-Nb_2N. The lattice constant, a, and the chemical composition of the NbC_xN_y as a complete solid solution of NbC and NbN was estimated using Vegard's law [33]. According to the Vegard's law, lattice constants and chemical compositions of the intermediate NbC_xN_y, have a linear relation from the NbC (JCPDS: 38-1364) to NbN (JCPDS: 38-1155). We used $NbC_{0.5}N_{0.5}$ powder (the lattice constant, a = 4.4305 Å) as a starting material. Fig. 1(b)–(e) shows the XRD profiles for the heat-treated $NbC_{0.5}N_{0.5}$ powders at the temperature range of 700–1000 °C in N_2 gas containing O_2 of 10^{-4} atm O_2 with holding time of 20 h. No Nb_2O_5 peaks were observed in the specimen heat-treated at

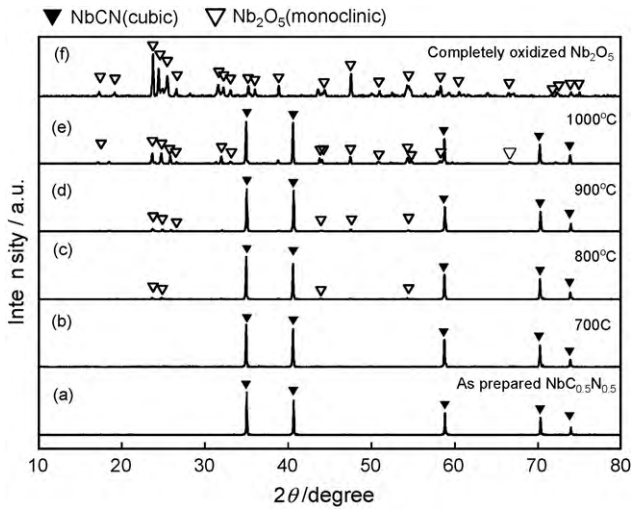

Fig. 1. XRD patterns of NbC_xN_y with and without heat-treatment under N_2 gas containing O_2 of 10^{-3}–10^{-4} atm O_2 at the temperature range of 700–1000 °C.

700 °C. Although the surface of the specimen was slightly oxidized, the oxide layers might be too thin to be detected by XRD. The Nb_2O_5 peaks were observed in the Nb-CNO powders heat-treated above 800 °C. The peak intensity of the Nb_2O_5 gradually increased with the increase in the heat treatment temperature. Because the flowing gas during the heat treatment contained a small amount of O_2, the partial oxidation of the $NbC_{0.5}N_{0.5}$ proceeded at higher temperature. However, as shown in Fig. 1(e) the oxide layer slightly grew up even under 1000 °C for 20 h because the partial pressure of O_2 (p_{O_2}) was low. In order to obtain the completely oxidized Nb_2O_5, the heat treatment was performed at 1000 °C for 20 h under p_{O_2} of 10^{-3} atm, which was one order of magnitude greater than 10^{-4} atm. The complete oxidation of the $NbC_{0.5}N_{0.5}$ proceeded under these conditions as shown in Fig. 1(f).

As described later, the highest ORR activity of the Nb-CNO at different heat treatment temperature with holding time of 20 h was obtained at 900 °C. Therefore, the effect of the holding time of heat treatment was examined at 900 °C. Fig. 2(b)–(f) shows the XRD patterns of Nb-CNO powders heat-treated under N_2 gas containing O_2 of 10^{-3} atm O_2 at 900 °C in the holding time from 10 to 50 h. Fig. 2(a) and (g) are the XRD patterns of $NbC_{0.5}N_{0.5}$ and Nb_2O_5, respectively. The peak intensity of the Nb_2O_5 was gradually increased with increasing the holding time. The color of powder changed from light-brownish yellow to light-black.

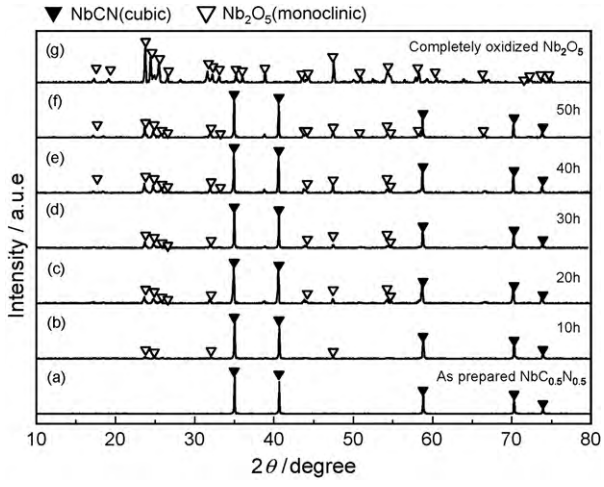

Fig. 2. XRD patterns of Nb-CNO powders heat-treated under N_2 gas containing O_2 of 10^{-3} atm O_2 at 900 °C in the holding time from 10 to 50 h.

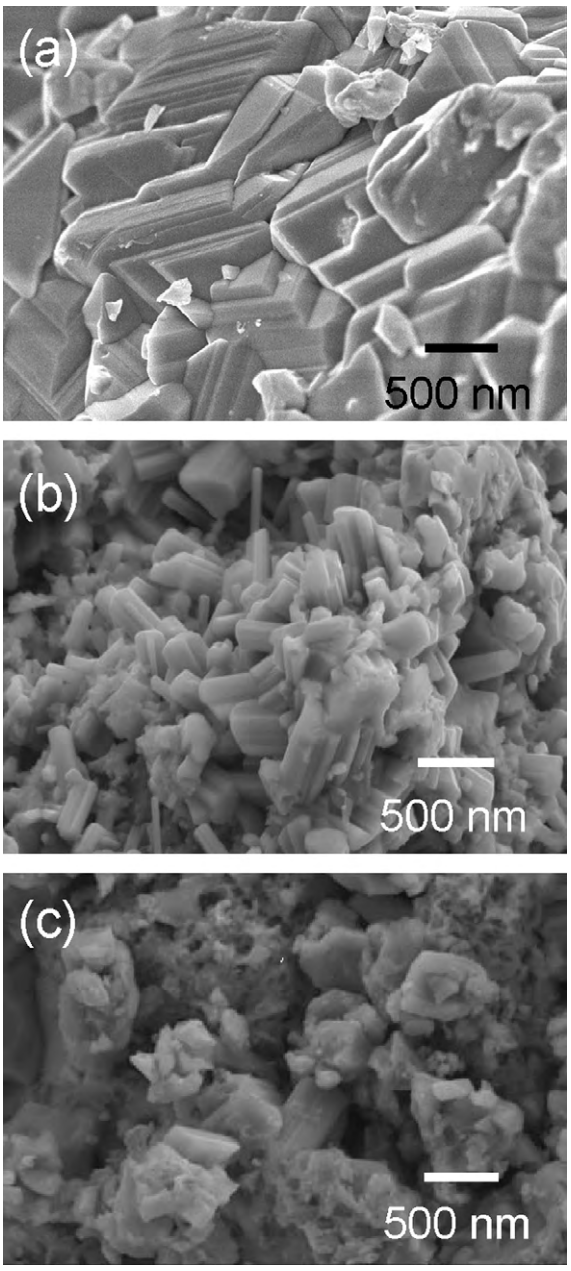

Fig. 3. SEM images of (a) $NbC_{0.5}N_{0.5}$ as a starting material (DOO = 0), (b) Nb-CNO partially oxidized at 900 °C under 10^{-4} atm O_2 for 20 h (DOO = 0.05), and (c) for 50 h (DOO = 0.21).

We define the degree of oxidation (DOO) of the $NbC_{0.5}N_{0.5}$ using the XRD spectra similar to Ta-CNO system as [28,30]:

$$\mathrm{DOO} = \frac{I(\mathrm{Nb_2O_5})}{I(\mathrm{NbC_xN_y}) + I(\mathrm{Nb_2O_5})} \quad (1)$$

where $I(NbC_xN_y)$ was the intensity of the maximum peak at $2\theta = 35°$ of NbC_xN_y and $I(Nb_2O_5)$ was the intensity of the maximum peak at $2\theta = 23.7°$ of Nb_2O_5. The specimen with DOO = 0 corresponded to the $NbC_{0.5}N_{0.5}$ and the specimen with DOO = 1 corresponded to the completely oxidized Nb_2O_5. The DOO of the Nb-CNO heat-treated at 700, 800, 900 and 1000 °C in N_2 gas containing O_2 of 10^{-4} atm for 20 h were 0, 0.03, 0.05 and 0.19, respectively. The DOO of the Nb-CNO heat-treated at 900 °C in 10^{-4} atm O_2 for 20, 25, 30, 40, and 50 h were 0.05, 0.06, 0.12, 0.18, and 0.21, respectively.

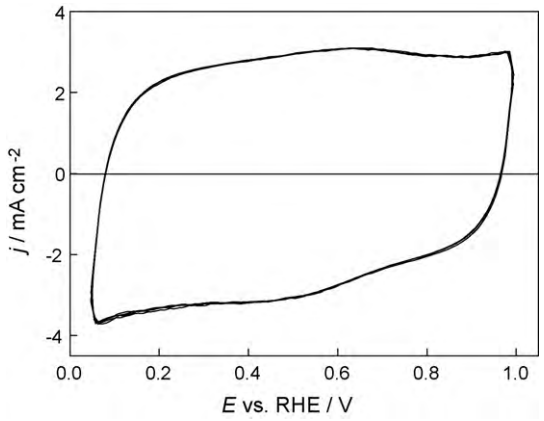

Fig. 4. Cyclic voltammogram of the Nb-CNO (DOO = 0.05), which was heat-treated at 900 °C for 20 h in N_2 gas containing O_2 of 10^{-4} atm, with the mixture of Ketjen Black with 5 wt.% in 0.1 mol dm^{-3} H_2SO_4 under N_2 at 30 °C.

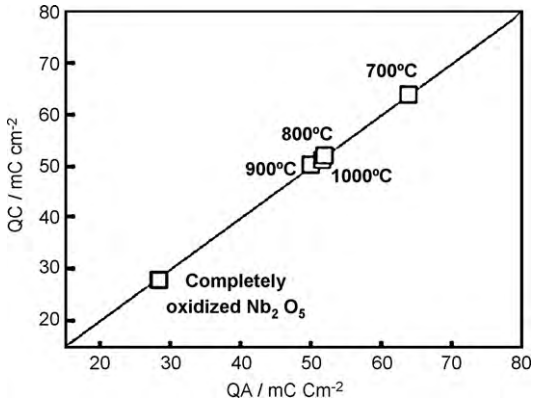

Fig. 5. Relationship between anodic and cathodic charges calculated from the CVs for the Nb-CNO powders partially oxidized at the temperature range of 700–1000 °C.

Fig. 3 shows the SEM images of the (a) $NbC_{0.5}N_{0.5}$ as a starting material (DOO = 0), (b) the Nb-CNO partially oxidized at 900 °C under 10^{-4} atm O_2 for 20 h (DOO = 0.05), and (c) for 50 h (DOO = 0.21). The $NbC_{0.5}N_{0.5}$ synthesized by a mixture of metal Nb and carbon black powder at 1500 °C in N_2 atmosphere shows the layered crystalline structure. The particle size of the $NbC_{0.5}N_{0.5}$ was several tens of micrometers. Tantalum and zirconium carbonitrides powders, which were synthesized by a mixture of oxide powders and carbon powder, had smaller particle sizes and such layered structure was not observed [28,29]. The $NbC_{0.5}N_{0.5}$ prepared by the mixture of metal Nb with carbon black was characterized by the large particle size and the layered structure. As shown in Fig. 3(b) and (c), the particle size and morphology of the partially oxidized $NbC_{0.5}N_{0.5}$ powders (DOO = 0.05 and 0.21) became more fine and rough than those of the starting material. This result was responsible for the progress of the partial oxidation.

3.2. Electrochemical stability and ORR activity

Fig. 4 shows a cyclic voltammogram (CV) of the Nb-CNO (DOO = 0.05), which was heat-treated at 900 °C for 20 h in N_2 gas containing O_2 of 10^{-4} atm, with the mixture of Ketjen Black with 5 wt.% in 0.1 mol dm^{-3} H_2SO_4 under N_2 at 30 °C. The Nb-CNO showed the quasi-rectangular shape of the CV. The shape of the CV was hardly changed after the potential cycle started and immediately reached the steady. No specific peaks due to an anodic dissolution were observed in the CV. This indicated that the Nb-CNO had a high electrochemical stability in an acid solution in the potential range from 0.05 to 1.0 V.

Fig. 5 shows the relationship between anodic and cathodic charges calculated from the CVs for the Nb-CNO powders partially oxidized at the temperature range of 700–1000 °C. If the Nb-CNO anodically dissolved, that is, the catalyst was unstable, the anodic charge was larger than the cathodic one. The anodic charges in the CV were corresponded to the cathodic ones in every CV. Therefore, these Nb-CNO powders have a high electrochemical stability in the potential range from 0.05 to 1.0 V.

Fig. 6 shows the potential–ORR current curves of the Nb-CNO powders partially oxidized at the temperature range from 700 to 1000 °C in 0.1 mol dm^{-3} H_2SO_4 at 30 °C with a scan rate of 5 mV s^{-1}. The curves of the as-prepared $NbC_{0.5}N_{0.5}$ (DOO = 0), the completely oxidized Nb_2O_5 (DOO = 1), Ketjen Black, and GC substrate were also shown. The ORR currents of the $NbC_{0.5}N_{0.5}$ and the Nb_2O_5 were observed below ca. 0.5 V. These currents were due to the Ketjen Black, indicating that the ORR activity of the $NbC_{0.5}N_{0.5}$ and the Nb_2O_5 was poor. On the other hand, the ORR current and the onset potential for the ORR increased with the increase in heat treatment temperature up to 900 °C, and then decreased. This result indicates that the catalytic activity for the ORR significantly depends on the heat treatment temperature, that is, degree of oxidation of the $NbC_{0.5}N_{0.5}$. Fig. 7 shows the dependence of the electrode potential at the $i_{ORR} = -0.2$ μA cm^{-2}, E_{ORR} (a), and the $|i_{ORR}|$ at 0.6 V (b) of the Nb-CNO powders heat-treated from 700 to 1000 °C for 20 h on the degree of oxidation of the $NbC_{0.5}N_{0.5}$. As shown in Fig. 7(a), the E_{ORR} of the as-prepared $NbC_{0.5}N_{0.5}$ (DOO = 0) without heat treatment was 0.61 V vs. RHE. The starting material had a low catalytic activity. On the other hand, the E_{ORR} of the Nb-CNO with heat treatment at 700 °C (DOO = 0) was 0.89 V. The E_{ORR} was abruptly increased by the heat treatment. Although the DOO calculated from the XRD patterns was the same, that is, DOO = 0, such a large difference of the E_{ORR} was observed. This was because the surface of the Nb-CNO at 700 °C was slightly oxidized, even no oxide peaks were observed in the XRD pattern. The slight oxidation of the catalyst surface would enhance the catalytic activity for the ORR. The Nb-CNO powders with the DOO from 0 to 0.19 had high constant value of the E_{ORR}. While, the completely oxidized Nb_2O_5 (DOO = 1) had lower E_{ORR}, Fig. 7(b) shows the dependence the $|i_{ORR}|$ at 0.6 V on the DOO. The $|i_{ORR}|$ at 0.6 V increased with the increasing DOO up to 0.05, and then decreased. Although the E_{ORR} hardly depended on the DOO, the $|i_{ORR}|$ at 0.6 V strongly depended on the DOO. This different behavior was probably responsible for the quality and quantity of the active site of the catalysts. The E_{ORR} and $|i_{ORR}|$ were mainly due to the quality and quantity of the active sites, respectively. The Nb-CNO

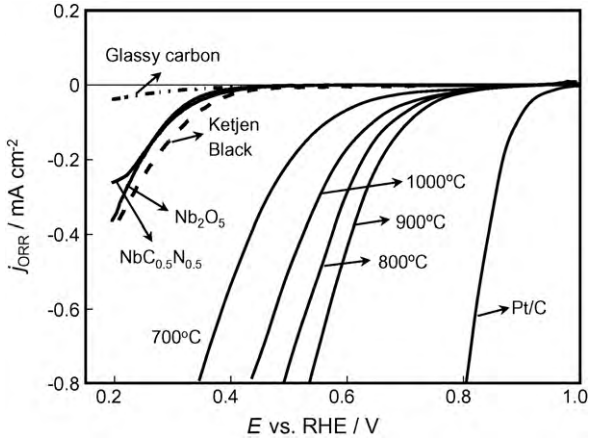

Fig. 6. Potential–ORR current curves of the Nb-CNO powders partially oxidized at the temperature range from 700 to 1000 °C in 0.1 mol dm^{-3} H_2SO_4 at 30 °C with a scan rate of 5 mV s^{-1}.

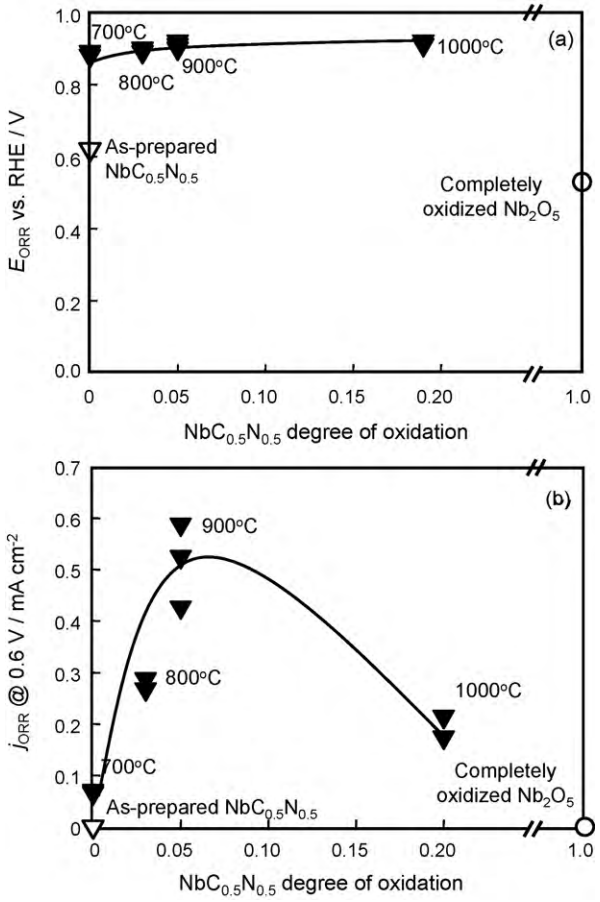

Fig. 7. Dependence of the electrode potential at the $i_{ORR} = -0.2\ \mu A\ cm^{-2}$, E_{ORR} (a), and the $|i_{ORR}|$ at 0.6 V (b) of the Nb-CNO powders heat-treated from 700 to 1000 °C for 20 h on the degree of oxidation of the $NbC_{0.5}N_{0.5}$.

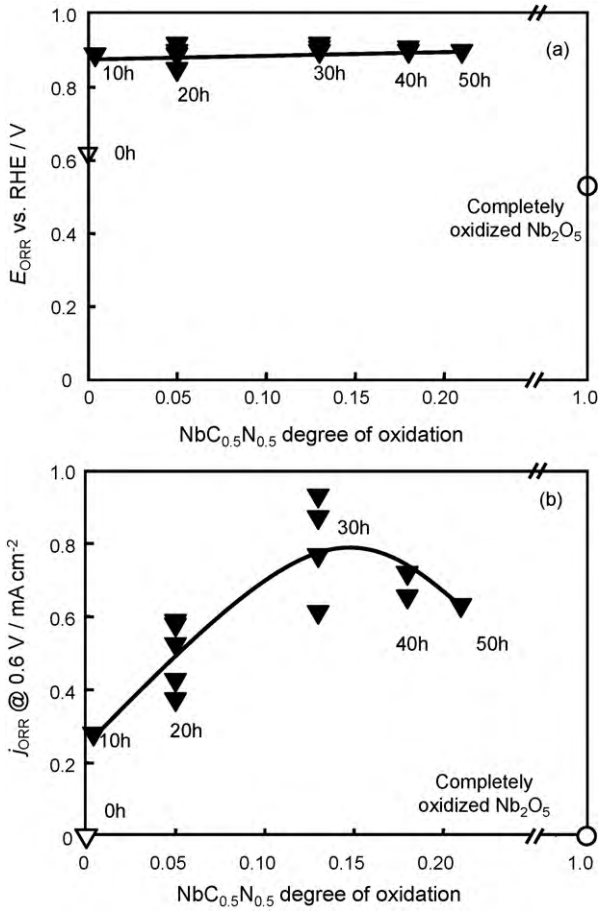

Fig. 8. Dependence of the electrode potential at the $i_{ORR} = -0.2\ \mu A\ cm^{-2}$, E_{ORR} (a), and the $|i_{ORR}|$ at 0.6 V (b) of the Nb-CNO powders heat-treated at 900 °C with the different holding time on the degree of oxidation of the $NbC_{0.5}N_{0.5}$.

powders had the same active site because of almost the same E_{ORR}. On the other hand, the quantity, that is, the density of the active sites on the surface had maximum around DOO of 0.05. The heat treatment temperature of 900 °C was suitable to obtain the high ORR activity with the holding time of 20 h. The effect of the holding time at 900 °C was examined to obtain the higher ORR activity.

Fig. 8 shows the dependence of the electrode potential at the $i_{ORR} = -0.2\ \mu A\ cm^{-2}$, E_{ORR} (a), and the $|i_{ORR}|$ at 0.6 V (b) of the Nb-CNO powders heat-treated at 900 °C with the different holding time on the degree of oxidation of the $NbC_{0.5}N_{0.5}$. The specimens with the DOO from 0.05 to 0.21 had high E_{ORR}, 0.9 V. The maximum of the E_{ORR} achieved at 0.92 V. The $|i_{ORR}|$ at 0.6 V had maximum in the specimen with the DOO of 0.13. Needless to say, the real surface area of the specimen was considered to evaluate the reaction current. However, it was difficult to estimate the real surface area of the specimen because small molecules such as H_2 and CO did not adsorb the surface. The electric charge calculated from the cyclic voltammetry could be used to estimate the real surface area of the working electrode. However, Ketjen Black was mixed with the Nb-CNO, the electric charge calculated from the cyclic voltammetry contained the large contribution of the Ketjen Black. When the contribution of the Ketjen Black was always the same, the electric charge calculated from the cyclic voltammetry reflected on the surface area of the Nb-CNO. From the viewpoint of real surface area, the Nb-CNO with heat-treated at 700 °C had largest surface area as shown in Fig. 5. However, the ORR current of the Nb-CNO with heat-treated at 700 °C was smallest among the specimens with different heat treatment temperature. Therefore, the increase in the ORR activity was responsible not the increase in the surface area but the increase in the density of the active site.

Therefore, the partial oxidation of the $NbC_{0.5}N_{0.5}$ was very useful to enhance the catalytic activity for the ORR. In addition, an appropriate oxidation of the $NbC_{0.5}N_{0.5}$ is essential to have a definite catalytic activity for the ORR. We found that partially oxidized tantalum and zirconium carbonitrides had definite catalytic activity for the ORR [28,29]. The Nb-CNO also had the catalytic activity for the ORR. Although the E_{ORR} of the Nb-CNO still was lower than 1.05 V vs. RHE of the commercial Pt/C (TKK; 46.3 wt.% Pt loading), the Nb-CNO might be one of the hopeful candidates as nonplatinum cathode for PEFCs.

3.3. Structural and electronic properties

The chemical bonding state of the surface was analyzed using an X-ray photoelectron spectroscopy (XPS). Fig. 9 shows the XPS spectra of the as-prepared $NbC_{0.5}N_{0.5}$, the Nb-CNO powders partially oxidized at 700 and 900 °C for 20 h under 10^{-4} atm O_2, and Nb_2O_5: Nb 3d (a), C 1s (b), O 1s (c), and N 1s (d) regions. The DOO of the Nb-CNO powders at 700 and 900 °C for 20 h were 0 and 0.05, respectively. As shown in Fig. 9(b) and (d), the as-prepared $NbC_{0.5}N_{0.5}$ had peaks identified as NbC (282.8 eV) [38] and NbN (397.2 eV) [39]. The binding energies of Nb $3d_{5/2}$ peaks corresponding to NbC and NbN were 203.7 eV [40] and 203.8 eV [41], respectively. Niobium forms oxides in various oxidation states, i.e., NbO_2 (Nb^{4+}) at a binding energy of 205.5–206.0 eV, and Nb_2O_5 (Nb^{5+}) at 207.0–207.6 eV [40,42]. Three peaks were superimposed in the Nb $3d_{5/2}$ spectrum

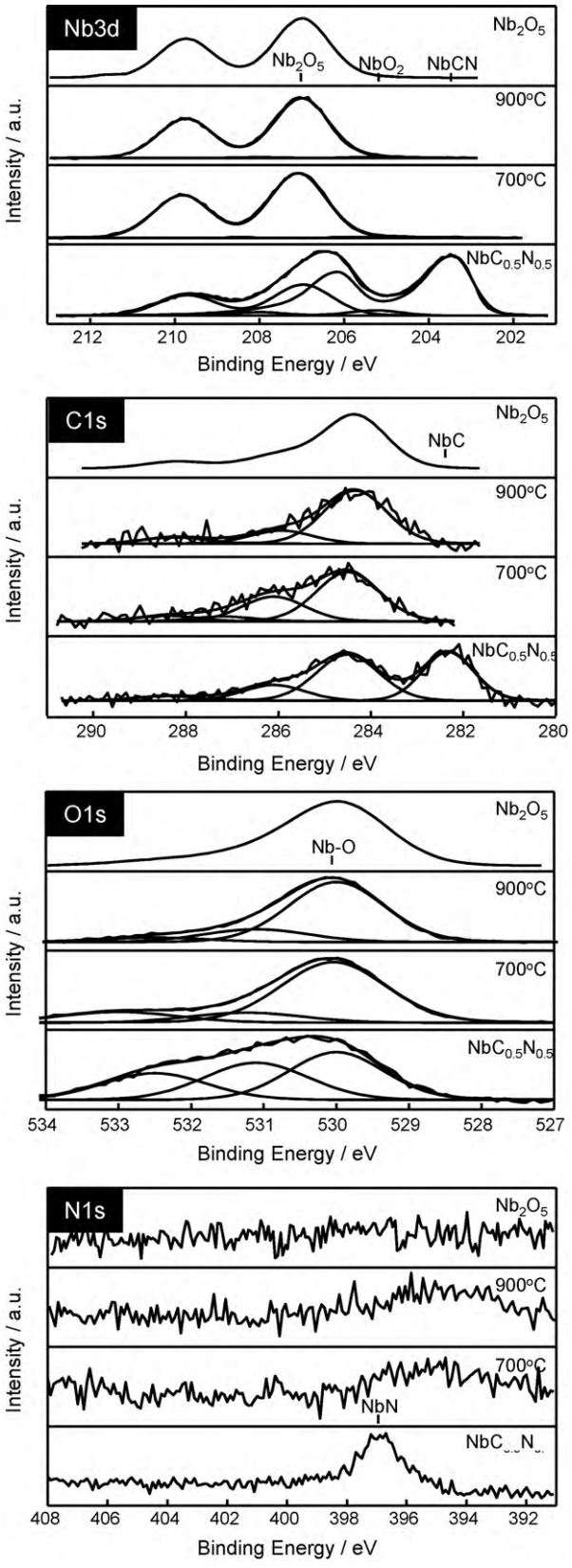

Fig. 9. XPS spectra of the as-prepared $NbC_{0.5}N_{0.5}$, the Nb-CNO powders partially oxidized at 700 and 900 °C for 20 h under 10^{-4} atm O_2, and Nb_2O_5: Nb 3d (a), C 1s (b), O 1s (c), and N 1s (d) regions.

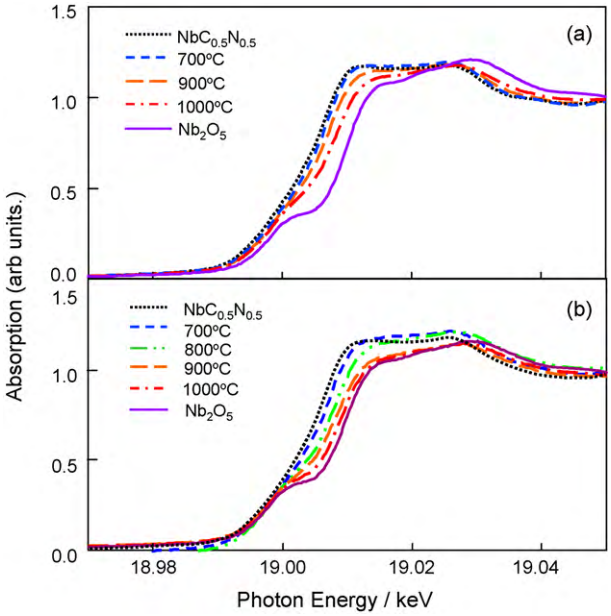

Fig. 10. Nb-K XANES spectra of the Nb-CNO powders partially oxidized at 700–1000 °C for 20 h under 10^{-4} atm O_2 taken in a transmission mode (a) and CEY mode (b).

of the $NbC_{0.5}N_{0.5}$. The first peak was positioned near the peak of NbC or NbN, and the second peak located at the peak of NbO_2 was very small. The third peak was identified as Nb_2O_5. This result indicated that the surface of the $NbC_{0.5}N_{0.5}$ was mainly composed of NbC_xN_y and Nb_2O_5. Although the XRD pattern of the $NbC_{0.5}N_{0.5}$ had only NbC_xN_y peaks, the surface of the $NbC_{0.5}N_{0.5}$ powder was partially oxidized in air and/or oxygen molecules adsorbed on the surface.

As shown in Fig. 1(b), the Nb-CNO partially oxidized at 700 °C for 20 h under 10^{-4} atm O_2 had also only NbC_xN_y peaks in the XRD pattern, that is, the DOO = 0. However, no peak due to NbC or NbN was observed in the Nb 3d, C 1s, and N 1s spectra. This result suggested that the surface of the Nb-CNO partially oxidized at 700 °C for 20 h was considerably oxidized. The XPS and XRD analyses indicated that the surface of the Nb-CNO partially oxidized at 700 °C for 20 h was oxidized, although the inner part of the specimen remained the carbonitride. Considering the drastic increase in the E_{ORR} between the as-prepared $NbC_{0.5}N_{0.5}$ and the Nb-CNO partially oxidized at 700 °C, the Nb compound with the highest oxidation state, that is, Nb_2O_5, enhanced the ORR activity. Ohnishi et al. also suggested that the Nb with the highest oxidation state would enhance the catalytic activity for the ORR based on the X-ray photoelectron spectra of the Nb oxide-based thin film prepared by reactive spattering [43]. The Nb-CNO partially oxidized at 900 °C for 20 h under 10^{-4} atm O_2 had almost the same XPS of the Nb-CNO partially oxidized at 700 °C, as shown in (a) Nb 3d, (b) C 1s, (c) O 1s, and (d) N 1s. The similar chemical bonding state of the surface supported that the E_{ORR} of both Nb-CNO powders had the same high value, ca. 0.9 V. However, these spectra of the partially oxidized specimens were also similar to those of the Nb_2O_5. There was a large difference of the E_{ORR} between the Nb-CNO powders and the Nb_2O_5. Such a difference of the E_{ORR} could not be explained by these XPS spectra. In addition, as shown in Fig. 7(a) and (b), although the E_{ORR} was the same, the $|i_{ORR}|$ at 0.6 V of the Nb-CNO partially oxidized at 900 °C was ca. 5–6 times greater than that of the Nb-CNO partially oxidized at 700 °C. No difference was observed in the XPS to explain such a large difference of the ORR current.

Fig. 10 shows the Nb-K XANES spectra of the Nb-CNO powders partially oxidized at 700–1000 °C for 20 h under 10^{-4} atm O_2 taken in a transmission mode (a) and CEY mode (b). We can see that

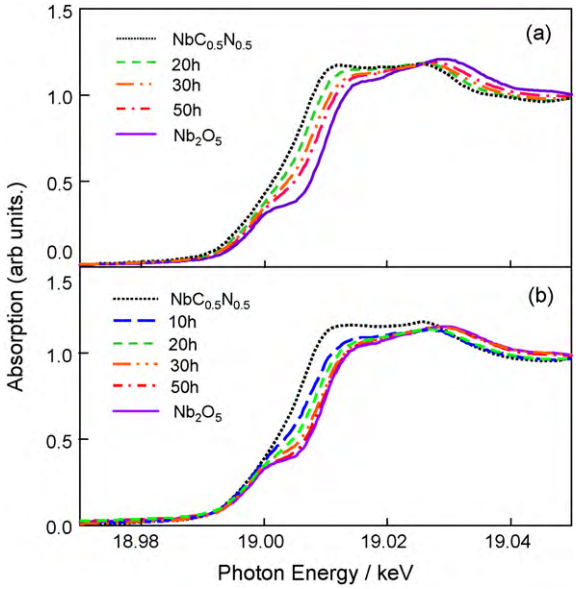

Fig. 11. Nb-K XANES spectra of the Nb-CNO powders partially oxidized at 900 °C for 20–50 h under 10^{-4} atm O_2 obtained in a transmission mode (a) and CEY mode (b).

the spectra of the partially oxidized $NbC_{0.5}N_{0.5}$ shifted to Nb_2O_5 with the increasing heat treatment temperature in both transmission and CEY mode. We note the shift in XANES spectra taken in the transmission mode was smaller than those obtained in the CEY mode. This difference can be explained by considering the difference of the probing depth: the transmission XAS probed the average characteristic of whole particles, while the CEY-XAS detected the near surface with the probing depth of 195 nm. Consequently, the contribution from surface oxides is rather dominant in CEY-XAS, giving rise to larger shift in the CEY-XAS spectra than those for the transmission XAS spectra. Since the CEY-XANES spectra for the most oxidized Nb-CNO prepared at 1000 °C still shows the contribution from NbC_xN_y cores, namely, the chemical shift is different from that of complete oxide, further EXAFS analysis do not work for this system. We will try this in the following system.

Fig. 11 shows the Nb-K XANES spectra of the Nb-CNO powders partially oxidized at 900 °C for 20–50 h under 10^{-4} atm O_2 obtained in a transmission mode (a) and CEY mode (b). In contrast with above case, now, the XANES spectra of the Nb-CNO powders in the CEY mode were almost identical to the complete oxide for the Nb-CNO powders heat-treated over 30 h, that is, the DOO above 0.18. This indicates that the surface oxide phase grows to a thickness that is larger than the probing depth (195 nm), and consequently, CEY-XAS could selectively detect the surface information with the exclusion of contribution from the NbC_xN_y cores.

Then, let us look at the local structure of these Nb-CNO specimens by EXAFS analyses. Fig. 12 exhibits the Fourier transforms of Nb-K EXAFS of the Nb-CNO partially oxidized at 900 °C for 40 h under 10^{-4} atm O_2 and Nb_2O_5 in the CEY mode. Interestingly, the clear difference was observed in the radial structure functions for the Nb-CNO partially oxidized at 900 °C for 40 h and the complete oxide, and this difference should be related with ORR active sites. In the crystalline structure of Nb_2O_5, 15 different Nb sites are present [44]. The peaks at around 0.16, 0.30, and 0.35 nm were attributed to Nb–O, Nb–(O)–Nb(1) and Nb–(O)–Nb(2) coordination, respectively [45]. Although a complete determination of the local structure is difficult to obtain due to the Nyquist's theorem restriction, the difference in the radial structure functions could be explained by considering oxygen vacancies similar to Ta-CNO powders [34]. However, further experiments and detailed analyses should be required to identify the active sites.

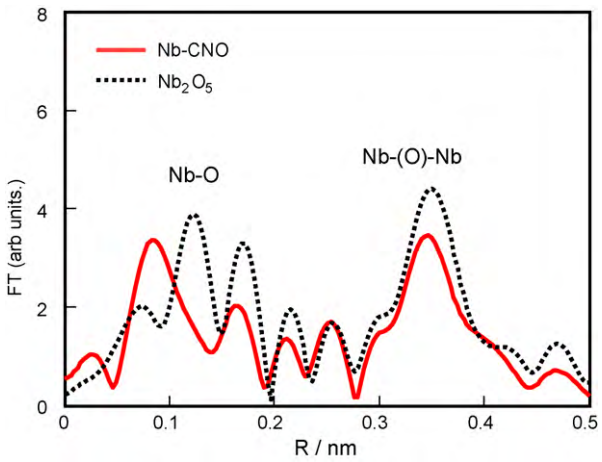

Fig. 12. Fourier transforms of Nb-K EXAFS of the $NbC_{0.5}N_{0.5}$ partially oxidized at 900 °C above 40 h under 10^{-4} atm O_2 and Nb_2O_5 in the CEY mode.

The ionization potential of the specimens was measured using a photoelectron spectrometer surface analyzer to reveal the difference of the surface electronic state between the Nb-CNO partially oxidized at 900 °C for 40 h under 10^{-4} atm O_2 and the Nb_2O_5. Fig. 13 shows the relationship between the square root of the photoelectric quantum yield $Y^{1/2}$ and the photon energy, that is, the photoelectron spectra of the specimens. The beam power was 200 nW. Because the $NbC_{0.5}N_{0.5}$ was an electrical conductor, the photoelectron was emitted at low photon energy, ca. 4.7 eV. The photoelectrons were difficult to emit with the progress of the oxidation. The square root of the photoelectric quantum yield increased linearly with increasing the photon energy on each specimen. The slope of the straight line reflected the tendency of the photoelectron emission of the specimens, that is, the density of state of the electrons near the Fermi level. The slope of the Nb_2O_5 was apparently lower than that of others, because Nb_2O_5 is an insulator. It is remarkable that the Nb-CNO partially oxidized at 900 °C for 40 h had higher slope than the Nb_2O_5. The slope of the Nb-CNO partially oxidized at 900 °C was similar to that of the $NbC_{0.5}N_{0.5}$, indicating that the Nb-CNO had larger electron energy levels than the Nb_2O_5 near the Fermi level. The intersection between the straight line and the background line in the photoelectron spectra provided a threshold energy. The threshold energy corresponded to a photoelectric ionization potential, which accorded with the work function in case

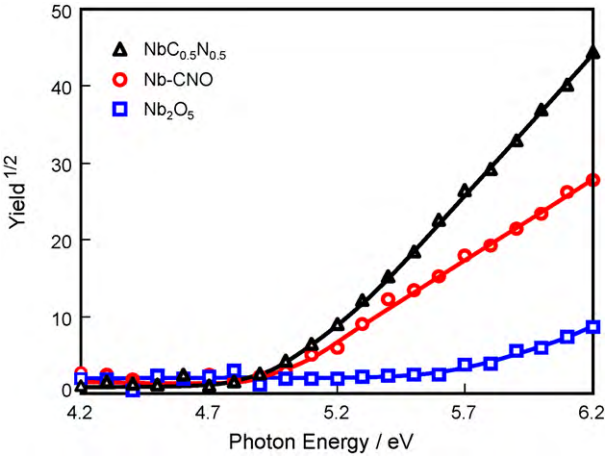

Fig. 13. Photoelectron spectra of the $NbC_{0.5}N_{0.5}$, the $NbC_{0.5}N_{0.5}$ partially oxidized at 900 °C for 40 h under 10^{-4} atm O_2, and the Nb_2O_5.

of metals. The ionization potential of the $NbC_{0.5}N_{0.5}$, the Nb-CNO partially oxidized at 900 °C for 40 h, and the commercial Nb_2O_5 was 4.98 eV, 4.99 eV, and 5.63 eV, respectively. The work function of metal Nb was 4.3 eV [46]. The ionization potential of the $NbC_{0.5}N_{0.5}$ was 0.6 eV larger than that of metal Nb, because of the carbonitridation. On the other hand, the highest energy level of electrons in the valence band of Nb_2O_5 is ca. −7.6 eV [47], that is, the ionization potential of Nb_2O_5 is predicted to be ca. 7.6 eV. However, the ionization potential of the commercial Nb_2O_5 was no less than ca. 2.0 eV lower than that predicted from literature. The surface level of the commercial Nb_2O_5 probably caused the lower ionization potential. Although the XRD and XPS analysis suggested that the physical properties such as the crystalline structure and the chemical bonding state of the surface of the Nb-CNO partially oxidized at 900 °C for 40 h was similar to those of the Nb_2O_5, the ionization potential and the density of state of the electrons near the Fermi level in these specimens was obviously different. The ionization potential obtained in this study was much lower than that of the commercial Nb_2O_5. Henrich et al. found that the work function of the oxides decreased with increasing the density of defects [48]. Therefore, the low ionization potential suggested that the Nb-CNO had some surface defects. Lattice defects and impurities introduce localized electron levels in the band gap of metal oxides. Vacancies of oxide ion give donor levels close to the edge level of the conduction band [49]. Therefore, we think that the Nb-CNO probably had some vacancies of oxide ion. The oxygen defects might be responsible for the oxygen reduction capability by creating electronically favorable oxygen adsorption sites.

4. Conclusions

The partially oxidized $NbC_{0.5}N_{0.5}$ (Nb-CNO) was investigated as non-platinum catalyst for the reduction of oxygen in acidic medium. $NbC_{0.5}N_{0.5}$ powder was synthesized from the mixture of metallic Nb powder and carbon black at 1500 °C in N_2 atmosphere. The $Nb_{0.5}N_{0.5}$ powders were heat-treated at the temperature range of 700–1000 °C in N_2 gas containing O_2 of 10^{-4} atm O_2. These specimens had Nb_2O_5 peaks as well as carbonitrides peaks in the XRD patterns. The onset potential for the ORR of the Nb-CNO achieved 0.92 V vs. RHE in 0.1 M H_2SO_4 at 30 °C, which was much higher than those of the completely oxidized Nb_2O_5 (0.53 V) and the as-prepared $NbC_{0.5}N_{0.5}$ (0.61 V). X-ray photoelectron spectra suggested that Nb_2O_5 on the surface was essential to have the catalytic activity for the ORR. The XPS and XRD analyses indicated that the surface of the heat-treated $NbC_{0.5}N_{0.5}$ was fairly oxidized and the inner part of the specimen remained the carbonitride. It was found that an appropriate surface oxidation of the $NbC_{0.5}N_{0.5}$ was essential to enhance the catalytic activity for the ORR. The EXAFS and the ionization potential measurement revealed that the oxide layer formed on the surface of the Nb-CNO had different local structure from Nb_2O_5 and probably had oxygen vacancy defects, which created the oxygen adsorption active sites.

Acknowledgements

This work was performed under the "Non-precious metal oxide-based cathode for PEFC Project" supported by the New Energy and Industrial Technology Development Organization (NEDO). The synchrotron experiments, the transmission XAS and CEY-XAS measurements, were carried out on the BL16B2 and BL14B2 beamlines at SPring-8 under approval from the Japan Synchrotron Radiation Institute (JASRI) (Proposal nos. 2008B5392, 2009A5391, 2009B5390, 2008A1892, 2008B1850, 2009A1803, and 2009B1821).

References

[1] A. Ishihara, S. Mitsushima, N. Kamiya, K. Ota, J. Power Sources 126 (2004) 34.
[2] D.M. Bernardi, M.W. Verbrugge, J. Electrochem. Soc. 139 (1992) 2477.
[3] Report on Trends for the Supply Demand of Platinum Group Metals for Fuel Cell Systems, Metal Economics Research Institute, Japan, 2005, p. 38 and 351 (in Japanese).
[4] The Motor Industry of Japan, Japan Automobile Manufactures Association Inc., 2005, p. 42.
[5] R. Jasinski, Nature 201 (1964) 1212.
[6] H. Jahnke, M. Schonborn, Comptes Rendus, Troisiemes Journees Internationalesd'Etude des Piles a Combustible 60 (1969) (Presses Academiques Europeennes, Bruxelles).
[7] C.W.B. Bezerra, L. Zhang, K. Lee, H. Liu, A.L.B. Marques, E.P. Marques, H. Wang, J. Zhang, Electrochim. Acta 53 (2008) 4937.
[8] J.H. Zagal, in: W. Vielstich, A. Lamm, H.A. Gasteiger (Eds.), Handbook of Fuel Cells—Fundamentals, Technology and Applications, vol. 2, John Wiley & Sons Ltd., West Sussex, 2003, p. 545.
[9] R. Bashyam, P. Zelenay, Nature 443 (2006) 63.
[10] M. Lefevre, E. Proietti, F. Jaouen, J.P. Dodelet, Science 324 (2009) 71.
[11] N. Alonso-Vante, H. Tributsch, Nature 323 (1986) 431.
[12] A. Lewera, J. Inukai, W.P. Zhou, D. Cao, H.T. Duong, N. Alonso-Vante, Electrochim. Acta 52 (2007) 5759.
[13] N. Alonso-Vante, in: W. Vielstich, A. Lamm, H.A. Gasteiger (Eds.), Handbook of Fuel Cells—Fundamentals, Technology and Applications, vol. 2, John Wiley & Sons Ltd., West Sussex, 2003, p. 534.
[14] K. Lee, A. Ishihara, S. Mitsushima, N. Kamiya, K. Ota, Electrochim. Acta 49 (2004) 3479.
[15] A. Ishihara, K. Lee, S. Doi, S. Mitsushima, N. Kamiya, M. Hara, K. Domen, K. Fukuda, K. Ota, Electrochem. Solid-State Lett. 8 (2005) A201.
[16] Y. Shibata, A. Ishihara, S. Mitsushima, N. Kamiya, K. Ota, Electrochem. Solid-State Lett. 10 (2007) B43.
[17] A. Ishihara, S. Doi, S. Mitsushima, K. Ota, Electrochim. Acta 53 (2008) 5442.
[18] Y. Ohgi, A. Ishihara, Y. Shibata, S. Mitsushima, K. Ota, Chem. Lett. 37 (2008) 608.
[19] Y. Liu, A. Ishihara, S. Mitsushima, N. Kamiya, K. Ota, Electrochem. Solid-State Lett. 8 (2005) A400.
[20] Y. Liu, A. Ishihara, S. Mitsushima, N. Kamiya, K. Ota, J. Electrochem. Soc. 154 (2007) B664.
[21] Y. Liu, A. Ishihara, S. Mitsushima, K. Ota, Electrochim. Acta 55 (2010) 1239.
[22] J.-H. Kim, A. Ishihara, S. Mitsushima, N. Kamiya, K. Ota, Electrochim. Acta 52 (2007) 2492.
[23] S. Doi, A. Ishihara, S. Mitsushima, N. Kamiya, K. Ota, J. Electrochem. Soc. 154 (2007) B362.
[24] Y. Maekawa, A. Ishihara, S. Mitsushima, K. Ota, Electrochem. Solid-State Lett. 11 (2008) B109.
[25] Y. Ohgi, A. Ishihara, K. Matsuzawa, S. Mitsushima, K. Ota, J. Electrochem. Soc. 157 (2010) B885.
[26] J.-H. Kim, A. Ishihara, S. Mitsushima, N. Kamiya, K. Ota, Chem. Lett. 36 (2007) 514.
[27] J.-H. Kim, A. Ishihara, S. Mitsushima, N. Kamiya, K. Ota, Electrochemistry 75 (2007) 166.
[28] A. Ishihara, Y. Shibata, S. Mitsushima, K. Ota, J. Electrochem. Soc. 155 (2008) B400.
[29] A. Ishihara, M. Tamura, K. Matsuzawa, S. Mitsushima, K. Ota, Electrochim. Acta, in press.
[30] A. Ishihara, M. Tamura, K. Matsuzawa, S. Mitsushima, K. Ota, J. Fuel Cell Sci. Technol., in press.
[31] A. Ishihara, Y. Ohgi, K. Matsuzawa, S. Mitsushima, K. Ota, Electrochim. Acta, in press.
[32] K.-D. Nam, A. Ishihara, K. Matsuzawa, S. Mitsushima, K. Ota, Electrochem. Solid-State Lett. 12 (2009) B158.
[33] P. Duwez, F. Odell, J. Electrochem. Soc. 97 (1950) 299.
[34] H. Imai, M. Matsumoto, T. Miyazaki, S. Fujieda, A. Ishihara, M. Tamura, K. Ota, Appl. Phys. Lett. 96 (2010) 191905.
[35] A. Erbil, G.S. Cargill, R. Frahm, F. Boehme, Phys. Rev. B 37 (1988) 2450.
[36] S.L. Schreder, Solid State Commun. 98 (1996) 405.
[37] H. Kirihata, M. Uda, Rev. Sci. Instrum. 52 (1981) 68.
[38] A. Bendavid, P.J. Martin, T.J. Kinder, E.W. Preston, Surf. Coat. Technol. 163–164 (2003) 347.
[39] D. Bekermann, D. Barreca, A. Gasparotto, H.W. Becker, R.A. Fischer, A. Devi, Surf. Coat. Technol. 204 (2009) 404.
[40] M.T. Marques, A.M. Ferraria, J.B. Correia, A.M. Botelho do Rego, R. Vilar, Mater. Chem. Phys. 109 (2008) 174.
[41] G. Jouve, C. Séverac, S. Cantacuzène, Thin Solid Films 287 (1996) 146.
[42] S. Martínez-Méndez, Y. Henríquez, O. Domínguez, L. D'Ornelas, H. Krentzien, J. Mol. Catal. A: Chem. 252 (2006) 226.
[43] R. Ohnishi, Y. Takahashi, A. Takagaki, J. Kubota, K. Domen, Chem. Lett. 37 (2008) 838.
[44] K. Kato, Acta Crystallogr. B32 (1976) 764.
[45] S. Kodama, N. Ichikuni, K.K. Bando, T. Hara, S. Shimazu, Appl. Catal. A: Gen. 343 (2008) 25.
[46] H.B. Michaelson, J. Appl. Phys. 48 (1977) 4729.
[47] W. Schmickler, J.W. Schultze, J.O'.M. Bockris, in: B.E. Conway, R.E. White (Eds.), Modern Aspects of Electrochemistry, vol. 17, Plenum, New York, 1986, p. 357.
[48] V.E. Henrich, G. Dresselhaus, H.J. Zeiger, Phys. Rev. Lett. 36 (1976) 1335.
[49] C. Stampfl, A.J. Freeman, Phys. Rev. B 67 (2003) 064108.